Carbide Composition and Stress Measurement in Ethylene Pyrolysis Tubes

K.J. Stevens[a,b], B. Ingham[b,c], M. Ryan[c], V. Luzin[d] and K. Cheong[e].

[a]*Quest Integrity NZL Ltd, P.O. Box 38-096, Lower Hutt, New Zealand*
[b]*The MacDiarmid Institute for Advanced Materials and Nanotechnology, P.O. Box 600, Wellington, New Zealand*
[c]*Industrial Research Ltd, P.O. Box 31-310, Lower Hutt, New Zealand*
[d]*Bragg Institute, Australian Nuclear Science and Technology Organisation, Private Bag 1, Menai, NSW 2234*
[e]*British Energy Generation Ltd, Barnett Way, Gloucester, GL4 3RS, United Kingdom*

Corresponding author: k.stevens@questintegrity.com

The powder diffraction beamline at the Australian Synchrotron has been used to identify the carbide phases and to determine that the radial phase distribution had a maximum of 34 weight percent carbide in a typical ex-service carburised ethylene pyrolysis tube. Neutron diffraction at the Kowari beamline at OPAL (Open Pool Australian Light water reactor) was used with un-sectioned tubes to measure room temperature stresses of 400 MPa at the inside region of a heavily carburised tube, in the austenite phase caused by coking, carbon diffusion and carbide growth at 900-1150 °C. Finite Element Analysis has been used to model the stress evolution during plant operation, and the relative importance of the competing damage mechanisms.

1. Introduction

Ethylene is important in the production of polyethylene, used in thin film packaging, piping and cable sheathing. It is produced by steam cracking of naptha, LPG or ethane at temperatures up to 1150°C at high flow velocities. Carburisation of ethylene pyrolysis tubes causes a loss in weldability, corrosion resistance and ductility as the carbides are brittle, and provides a source of micro-cracking [1]. Plant operators prefer to replace tubes at planned outages and are interested in remaining life assessments assisted by description and modelling of the progress of carburisation. Table 1 shows the nominal HPM tube alloy composition before in-service exposure. Eddy current measurements have been taken on ex-service tubes, and there is a clear correlation between carburisation and an increase in magnetic permeability [2], but the calibration method used relies on understanding the microstructural origins of the magnetic properties. Life assessments rely on understanding the stress evolution in the tubes as a function of operating conditions. In this paper microstructural characterisation and stress measurement results for one representative carburised tube are presented.

Table 1: Tube alloy composition (nominal as received in wt%).

Tube Number	Alloy	Cr (%)	Fe (%)	Ni (%)	Ti (%)	Mn (%)	Mo (%)	Si (%)	P (%)	S (%)	C (%)
1-26-O	HPM nominal	23-26	Bal.	37-40	0.2-0.6	<=1.50	1.0-3.0	1.4-2.0	<=0.02	<=0.03	0.1-0.2

2. Results

2.1 Synchrotron X-ray Diffraction Carbide Phase Fraction Analysis

The synchrotron measurements were made on the powder diffraction beamline at the Australian synchrotron using 15.02 keV (0.825882 Å wavelength) X-rays. Sample sections were cut from 24 ex-service tubes, and mounted in bakelite moulds and polished to 1 micron, with the results from 1 tube only presented here. The X-ray beam was confined using slits to 1 mm vertically which was oriented with the radial direction of the samples. The beam spilled across about 5 mm in the sample circumferential or hoop direction. The samples were scanned across the beam to produce radial carbide phase fraction results.

The raw data were processed and output as ASCII xy data files. These were subsequently imported into Bruker Diffrac-plus EVA [3] software at Industrial Research Limited, for manual peak identification using the Powder Diffraction File database [4]. Bruker TOPAS v2.0 [5] was used for whole profile peak fitting [6], as shown in Figure 1, in order to determine the phase composition and to separate out peak broadening due to crystal grain size from instrumental effects [7]. The main phases included in the fitting were austenite, $Cr_{23}C_6$, Cr_7C_3, Cr_3C_2 and $(Fe\text{-}Mo)_6C$. LaB_6 powder was used for wavelength calibration and determination of instrumental parameters. The diffraction peaks were fit with a pseudo-Voigt profile. The lattice constants and peak widths were treated as fit variables in TOPAS, but the atom positions and space groups were taken from literature values for $M_{23}C_6$ [8], M_7C_3 [9], Cr_3C_2 [10] and M_6C [11]. The site occupancies and Debye-Waller temperature factors for each phase were constants. Figure 2 shows the phase fraction profile resulting from 8 fits to scans across a tube.

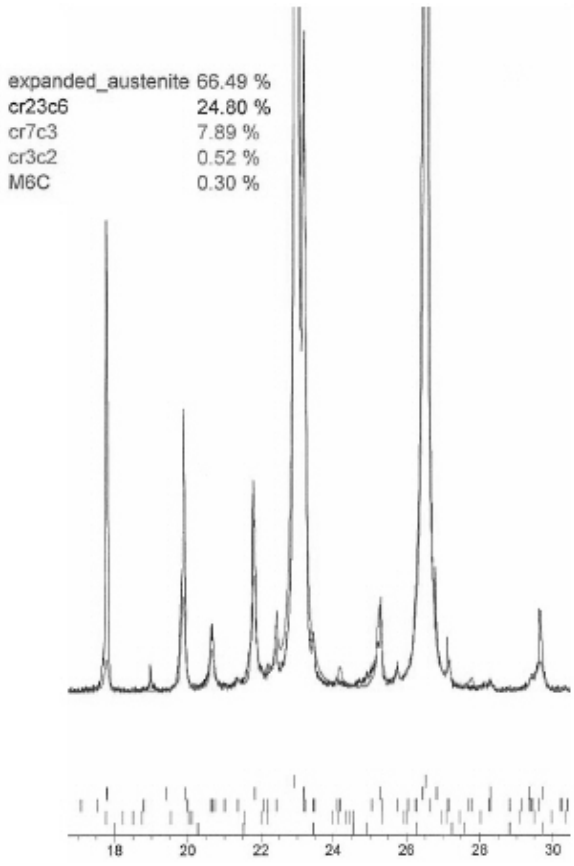

Fig. 1: TOPAS fit to a heavily carburised HPM alloy tube (1-26-O) at the inner diameter (the 1 mm position in Fig. 2). The dark line is the experimental linescan (an expanded region only is shown around the (111) and (200) peaks of austenite, but the fits were made on a data set from 8° to 90°), and the light grey line is the combined fit from austenite and 4 carbide phases. The vertical lines at the bottom of the figure show the peak positions in the same order as shown in the legend.

Due to the elastic anisotropy of the original HPM alloy, carbide formation strains the HPM anisotropically, which is observed as peak shifts corresponding to non-uniform changes in the lattice spacing. This has been observed previously in austenite expanded by nitridation or carburisation [12]. With increasing 2θ angle the diffracting planes have an increasing inclination to the sample normal, and a bi-axial stress in the plane of the sample thus has an increasing influence on the peak shift [13]. However a simple plane bi-axial stress model is insufficient to explain the observed austenite peak shifts, which indicates a stress gradient normal to the surface or the effects of elastic anisotropy. In order to account for these peak shifts, a "th2_offset" that is dependent on the h, k, l Miller indices of each peak has been applied using TOPAS. Due to the improved fit of the model to the data this has significantly improved the refinement residual, R_{wp}. The patterns from some samples also exhibited texture, and it was not possible to accurately quantify the phase profiles in those samples.

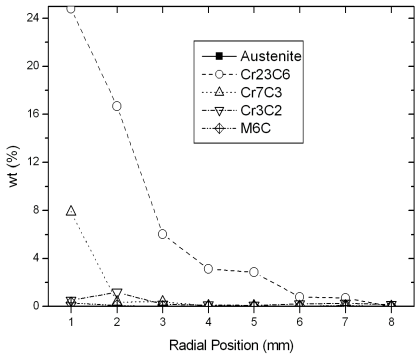

Fig. 2: Radial carbide relative fraction results for tube 1-26-O (remainder is austenite).

2.2 Neutron Diffraction Residual Stress Measurement

The Kowari beamline at the Australian Research Reactor (OPAL) was used for residual stress measurements at room temperature. Neutrons have a deeper penetration than X-rays and so neutron diffraction measurements of strain are more representative of the bulk [14]. The neutron wavelength was 1.706 Å, and the austenite (311) peak shift was monitored for stress measurement. The hoop and axial stress profiles are shown in Figure 3(a), for the same heavily carburised tube discussed in section 2.1.

Abaqus CAE 6.9.1 was used for Finite Element modelling of the stress profiles with the results shown in Figure 3(b). The 9 mm wall thickness, 28 mm inside radius tube was subdivided into 1 mm thick radial slices to match the 1 mm width X-ray spot used at the synchrotron. The materials properties for the elements in each slice were randomly assigned to either carbide or hpm alloy using a Fortran Abaqus user subroutine, but with an overall distribution calculated from the X-ray diffraction carbide fraction fits. Literature material property values for HPM alloy [15] and the pure carbide phase data [16-20] were used when available with general static brick C3D8R elements from the Abaqus standard library. An internal pressure of 3.25 atmospheres was applied. The temperature distribution was 870 °C on the outside surface and 850 °C on the inside surface.

The FEA modelled stresses are lower than the measured stresses illustrated in Fig. 3, but this is mainly because the initial model only included the growth of 2 mm of coke on the tube inside at elevated temperature, followed by 1 decoke cycle at 750 °C, before heating back to 850 °C. Typical plants go through a decoke cycle every 40 days, with each cycle inducing plasticity into the tube as the tube shrinks about a coke [21] shell with lower thermal expansion coefficient. The plasticity accumulates to give higher stresses and creep ductility exhaustion during longer periods of operation and repeated decoke cycles [1]. The initial model needs to be improved to incorporate stress relaxation by creep, and include carbon

diffusion and carbide growth at elevated temperature, which causes local compression of the austenite. This is being attempted using ABAQUS user subroutines to grow a carbide geometry within a crystal plasticity formalism that can more accurately include the microstructure.

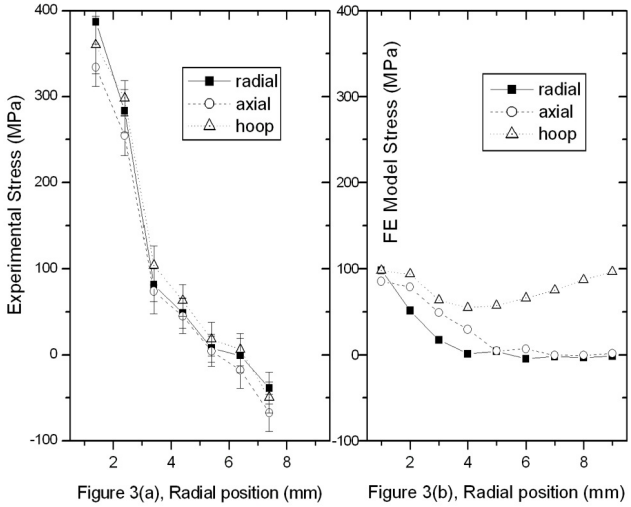

Fig. 3: Plot of residual stress (a) measurements and (b) model for tube 1-26-O.

Acknowledgements

This research was funded by NZ FRST IRL contract C08X0409 "Multiscale Modelling". Portions of this research was undertaken on the powder diffraction beamline at the Australian Synchrotron, Victoria, Australia.

References

[1] Jakobi D and Gommans R 2003 *Materials and Corrosion* **54** 881
[2] Stevens K and Trompetter W 2004 *J. Phys. D: Appl. Physics* **37** 501
[3] http://www.bruker-axs.de/eva.html
[4] http://www.icdd.com/index.htm
[5] http://www.bruker-axs.de/topas.html
[6] Coelho A A 2000 *J. Appl. Cryst*. **33** 899
[7] Sabine T M, Kennedy B J, Garrett R F, Foran G J and Cookson D J 1995 *J. Appl. Cryst.* **28** 513
[8] Bowman A L, Arnold G P, Storms E K and Nereson N G 1972 *Acta Cryst*. **B28** 3102
[9] Roualt A, Herpin P and Fruchart R 1970 *Ann. Chim*. **5** 461
[10] Pearson W B, "A Handbook of lattice spacings and structures of metals and alloys", Oxford, Pergamon, 1964
[11] Westgren A 1933 *Jernkont. Ann*. **117** 1
[12] Blawert C, Kalvelage H, Mordike B L, Collins G A, Short K T, Jirásková Y, Schneeweiss O 2001 *Surface and Coatings Technology* **136** 181
[13] Noyan I C and Cohen J B, 1986 "Residual Stress, Measurement by Diffraction and Interpetation", Springer-Verlag
[14] Hutchings M T, Withers P J, Holden T M, Lorentzen T 2005 "Introduction to the characterization residual stress by neutron diffraction", CRC Press.
[15] Metals Handbook, Vol. 3
[16] Antonov M and Hussainova I 2006 *Proc. Estonian Acad. Sci. Eng*. **12** 358
[17] DeSorbo W 1953 *J. Am. Chem. Soc*. **75** 1825
[18] Ershov V M 1984 *USSR Steel Journal*, English translation.
[19] Hussainova I et al. 2008 *Advances in Powder Metallurgy and Particulate Materials* .
[20] Jing C 2008 *Applied Phys. Lett*. **92**
[21] Smithells C J 1976 "Metals Reference Book", 5th edition, Butterworths, London